Available online at www.sciencedirect.com
ScienceDirect
Green Energy & Environment xxx (xxxx) xxx
www.keaipublishing.com/gee

Research Paper

Design of multifunctional interfaces on ceramic solid electrolytes for high-performance lithium-air batteries

Yunxin Shi [a], Ziyang Guo [a,b,*], Changhong Wang [b,d], Mingze Gao [a], Xiaoting Lin [b], Hui Duan [b], Yonggang Wang [a,c], Xueliang Sun [b,d,*]

[a] College of Energy Material and Chemistry, College of Chemistry and Chemical Engineering, Inner Mongolia University, Hohhot, 010021, China
[b] Department of Mechanical and Materials Engineering, Western University, London, ON, N6A 5B9, Canada
[c] Department of Chemistry and Shanghai Key Laboratory of Molecular Catalysis and Innovative Materials, Institute of New Energy, iChEM (Collaborative Innovation Center of Chemistry for Energy Materials), Fudan University, Shanghai, 200433, China
[d] Eastern Institute for Advanced Study, Eastern Institute of Technology, Ningbo, Zhejiang, 315100, China

Received 9 January 2024; revised 20 February 2024; accepted 28 February 2024
Available online ■ ■ ■

Abstract

High-energy-density lithium (Li)–air cells have been considered a promising energy-storage system, but the liquid electrolyte-related safety and side-reaction problems seriously hinder their development. To address these above issues, solid-state Li–air batteries have been widely developed. However, many commonly-used solid electrolytes generally face huge interface impedance in Li–air cells and also show poor stability towards ambient air/Li electrodes. Herein, we fabricate a differentiating surface-regulated ceramic-based composite electrolyte (DSCCE) by constructing disparately LiI-containing polymethyl methacrylate (PMMA) coating and Poly (vinylidene fluoride-co-hexafluoropropylene) (PVDF-HFP) layer on both sides of $Li_{1.5}Al_{0.5}Ge_{1.5}(PO_4)_3$ (LAGP). The cathode-friendly LiI/PMMA layer displays excellent stability towards O_2^- and also greatly reduces the decomposition voltage of discharge products in Li–air system. Additionally, the anode-friendly PVDF-HFP coating shows low-resistance properties towards anodes. Moreover, Li dendrite/passivation derived from liquid electrolyte-induced side reactions and air/I-attacking can be obviously suppressed by the uniform and compact composite framework. As a result, the DSCCE-based Li–air batteries possess high capacity/low voltage polarization (11,836 mA h g^{-1}/1.45 V under 500 mA g^{-1}), good rate performance (capacity ratio under 1000 mA g^{-1}/250 mA g^{-1} is 68.2%) and long-term stable cell operation (~300 cycles at 750 mA g^{-1} with 750 mAh g^{-1}) in ambient air.

Keywords: Li–air batteries; $Li_{1.5}Al_{0.5}Ge_{1.5}(PO_4)_3$; Polymers; Composite electrolyte; Ambient air

1. Introduction

With the rapid development of battery technology, the energy density of the current lithium (Li) ion cells is approaching their theoretical limit, but it is still difficult for them to meet the ballooning need of large-capacity power in portable electronics and electric transport equipment [1–8]. To address the above dilemma, developing the next-generation advanced batteries is extremely essential [9–16]. Among a series of new-type battery candidates, the Li–air system with ultra-high theoretical energy may win out in the future [17–19]. Nevertheless, many critical technical issues, including volatilization, leakage, decomposition of electrolytes, dendritic/passivated Li and the corresponding safety problems, need to be solved before practical applications of the Li–air cells outside the lab [20–24]. Most of these serious challenges are mainly related to

* Corresponding authors. Department of Mechanical and Materials Engineering, Western University, London, ON, N6A 5B9, Canada.
E-mail addresses: zyguo@imu.edu.cn (Z. Guo), xsun9@uwo.ca (X. Sun).

https://doi.org/10.1016/j.gee.2024.02.010

the widely used organic liquid electrolyte in the Li–air system [25–27]. Seeking new-type electrolytes to replace the liquid electrolyte is essential for the development of the Li–air batteries.

In response, developing solid-state electrolytes (SSE) has been considered as the optimal strategy to circumvent the above disadvantages [28–32]. Although the polymer-based SSEs have been widely investigated in Li-ion batteries, their low ionic conductivity at room temperature seriously retards their application in the Li–air cells [33–37]. Recently, inorganic solid electrolytes, such as sulfide, halide, or oxide-based SSEs, have attracted a great deal of attention due to their relatively high ionic conductivity [38–43]. Among them, the ceramic oxide-based SSEs, especially for $Li_{1.5}Al_{0.5}Ge_{1.5}(PO_4)_3$ (LAGP), exhibited great potential value in the Li–air batteries because of their high stability towards air, good ionic conductivity and wide voltage window [44–46]. Unfortunately, the high interface impedances between the ceramic electrolyte and electrodes seriously suppress the battery performance [47,48]. Moreover, it should be noted that the requirements of cathode and anode in Li metal batteries for the SSE interfaces are usually very different. For example, the SSEs possessing a highly stable surface towards reduction reaction are beneficial to Li anodes, while the SSEs with the superior oxidation-resistance surface are generally good for cathodes [49]. More importantly, for the open-structure Li–air system, the air cathodes not only face the high-voltage oxidation, but also are attacked by H_2O/O_2 in ambient air and O-based intermediates, which makes its requirements for the SSE interfaces more obviously different from these of Li anodes. In general, it is almost impossible for the single SSE to simultaneously meet the interface requirements of both electrodes in the Li–air batteries [47]. Very recently, the differentiated surface modification method has been developed and applied in solid-state Li metal batteries, which greatly improves the corresponding battery performances [47,49]. The above strategy may effectively address the critical problems of the current SSE-based Li–air cells. Hence, rationally designing the disparately modified layers on the ceramic electrolyte is of great significance for high-performance SSE-based Li–air batteries.

Herein, the differentiating surface-regulated ceramic-based composite electrolyte (DSCCE) is developed and further applied in Li–air batteries. Especially, the LiI-containing polymethyl methacrylate (PMMA) polymer and Poly (vinylidene fluoride-co-hexafluoropropylene) (PVDF-HFP) gel are coated on the LAGP pellet as the cathode-friendly and anode-friendly interfacial layers, respectively. The LiI-containing PMMA coating layer at the air cathode side can not only shows superior resistance towards superoxide intermediate but also effectively promotes the decomposition of discharge products at low overpotentials. Additionally, the PVDF-HFP modified layer can greatly reduce the interface impedances of the LAGP and further provide the tight contact surface with Li anode. Moreover, the compact LAGP ceramic electrolyte possesses the single Li-ion conductor behavior and also greatly suppress the air/O_2^- and redox mediator (RM) shuttling. As a result, the DSCCE-based Li–air batteries displayed excellent electrochemical properties when operated in ambient air, including the high discharge capacity, very low charge overpotential, and long cycle life with good safety.

2. Experimental section

2.1. DSCCE preparation

Firstly, the LAGP films were prepared according to our previous work [50]. Specifically, the polyvinyl butyral (PVA) was dissolved into the water to form 1 wt% PVA solution. Subsequently, the LAGP powders were uniformly mixed with PVA through the grinding method. After that, the obtained LAGP/PVA powders were pressed to form the pallets with the diameter of 12 mm (PVA can be used as binder to uniformly mix with solid electrolyte powder to make sure the LAGP powder easily being pressed into pellets at certain pressure condition) and further sintered at 950 °C for 6 h. Because of the fact that the content of PVA additives is very limited (less than 0.1 wt% of the LAGP/PVA powders), the emission of CO_2 gas derived from PVA decomposition is very low and thus the corresponding pores caused by CO_2 emission are also limited. Subsequently, two disparate-polymer coatings were fabricated through ultra violet (UV)-curable strategy on the both sides of LAGP film (wavelength of UV irradiation is 365 nm): on the air cathode side, the PMMA-based polymer layer was coated on LAGP through simply dropping precursor (which is made up of 1.0 mol L^{-1} bis (trifluoromethane) sulfonamide lithium salt (LiTFSI) in tetraglyme (TEGDME) containing 0.05 mol L^{-1} LiI (A), PMMA/Nmethyl-2-pyrrolidinone (NMP) (m/m: 1/4, B) with 2-hydroxy-2-methyl-1-phenyl-1-propanone (HMPP)/Trimethylolpropaneethoxylate-triacrylate (TMPET) (m/m: 0.01/3, C) by the mass ratio of 4:5:3) on its surface and further treated with the UV irradiating for about 30 s. For the anode side, the anode-friendly PVDF-HFP based polymer layer was constructed onto LAGP by the similar method (just using solution A without LiI and replacing PVDF-HFP with PMMA in solution B). Finally, the differentiatingly surface-regulated ceramic-based composite electrolyte (DSCCE) is synthesized and further store in the Ar-filled glovebox. The areal mass of the DSCCE electrolyte is ~150 mg cm^{-2}. In addition, the PVDF-HFP-based symmetrical polymer coating ceramic-based composite electrolyte (SPCCE) is also prepared by coating PVDF-HFP-based layers on the both sides of LAGP through the similar method.

2.2. Assembly of the DSCCE/SPCCE or LE based symmetrical or Li–air batteries and their electrochemical measurements

Firstly, the Li/SPCCE or commercial separator dipped with 1.0 mol L^{-1} LiTFSI in TEGDME/Li were orderly sealed into coin cells to fabricate the symmetric batteries in the glovebox filled with pure Ar. On the other hand, the Li–air full cells were assembled through using CNTs-based electrode (the preparation process is shown in supporting information) as catalytic cathodes, Li film as anodes and 1.0 mol L^{-1} LiTFSI/TEGDME dipped Celegard or DSCCE as electrolyte in the

Please cite this article as: Y. Shi et al., Design of multifunctional interfaces on ceramic solid electrolytes for high-performance lithium-air batteries, Green Energy & Environment, https://doi.org/10.1016/j.gee.2024.02.010

home-made Swagelok batteries. The amount of the liquid electrolyte (LE) added into a Li-air battery for comparison is ~100 μL. All the above batteries were further operated with the LAND testing system (Wuhan Land Electronic Co. Ltd). Moreover, other electrochemical tests, materials/electrode preparation and characterizations have also been summarized in supporting information.

3. Results and discussion

The differentiating surface-regulated ceramic-based composite electrolyte (DSCCE) is prepared through the solid-state sintered strategy followed by an in situ photopolymerization method. As illustrated in Fig. 1a, the as-prepared LAGP powders were firstly mixed with polyvinyl butyral (PVA) and pressed into the pellets under 30 MPa, which were subsequently sintered at a high temperature to obtain the LAGP ceramic. The LiI-containing polymethyl methacrylate (PMMA) and Poly (vinylidene fluoride-co-hexafluoro propylene) (PVDF-HFP) based gel polymer electrolyte were uniformly coated on LAGP film through ultraviolet solidification technology, respectively (Please see the experimental section for detail). The *in-situ* formed PVDF-HFP-based gel coating between LAGP and metallic Li can greatly suppress the potential side reaction and also reduce the interfacial resistance with Li electrodes, while the LiI-containing PMMA-based polymer layer is beneficial to O_2-related reaction around the air cathode. The detailed surface and cross-section morphology of DSCCE is studied through scanning electron microscopy (SEM) technology. There are two different surface coatings on DSCCE: the PMMA-based surface shows a buff color (due to the existence of I_3^-), while the PVDF-HFP-based coating displays a white surface color (Insert images of Fig. 1b and c). Although both coating layers

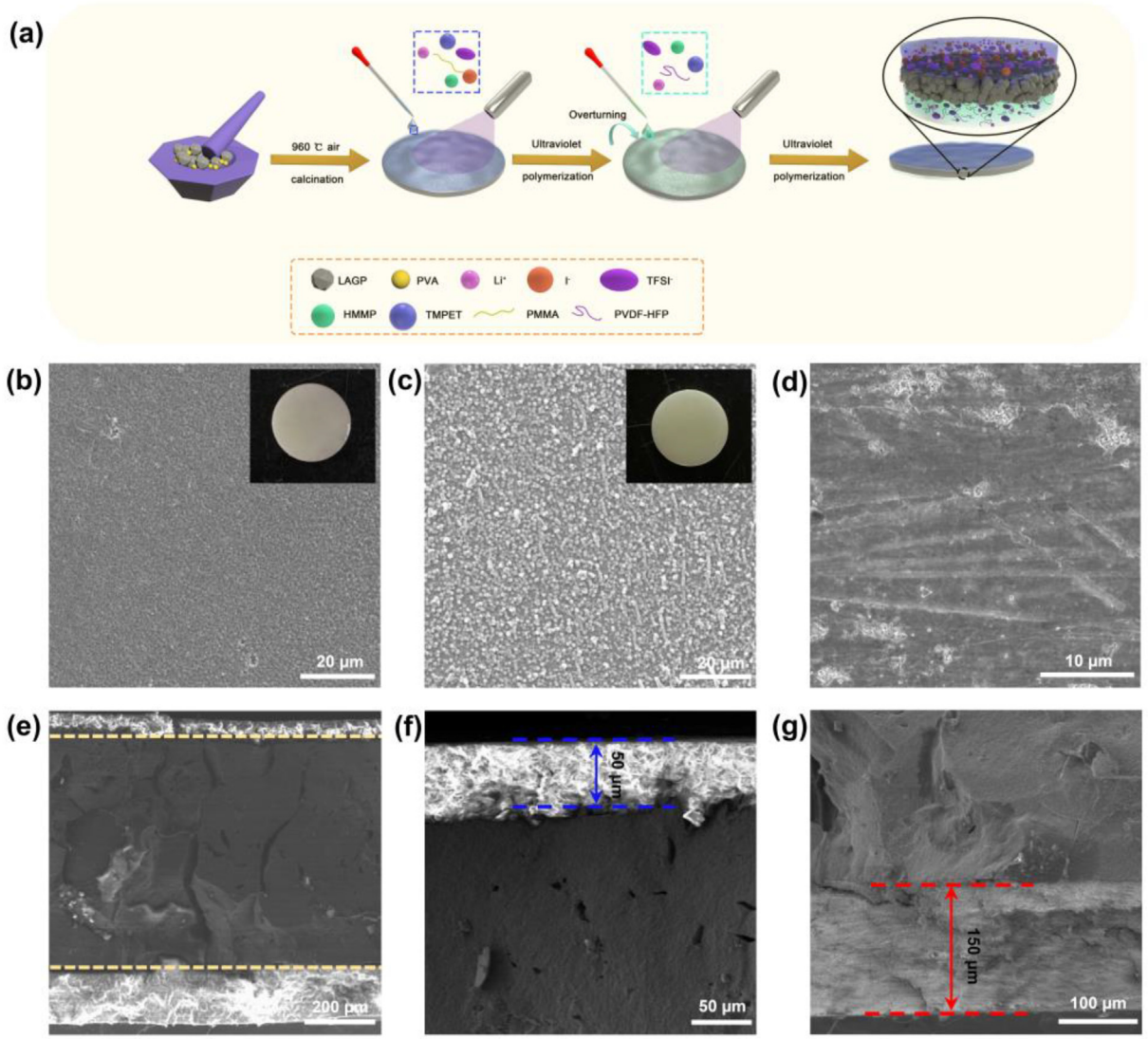

Fig. 1. (a) Schematic image of the preparation process for DSCCE; The surface SEM images and corresponding insert photographs of the (b) PVDF-HFP-based coating and (c) PMMA-based coating; (d) Surface SEM image of LAGP film; (e) Cross-sectional SEM image of DSCCE and its detailed cross-sectional images at different zones: (f) PVDF-HFP-based coating side and (g) PMMA-based coating side.

Please cite this article as: Y. Shi et al., Design of multifunctional interfaces on ceramic solid electrolytes for high-performance lithium-air batteries, Green Energy & Environment, https://doi.org/10.1016/j.gee.2024.02.010

on the LAGP film present a compact surface structure, the PMMA-based coating is mainly made up of uniform nanorods, which are different from the even particles in the PVDF-HFP-based layer (Fig. 1b and c). Compared with the PMMA or PVDF-HFP-based layer, the surface of LAGP seems to be more compact and denser (Fig. 1d), which should be beneficial to inhibit the shuttle of air. The X-ray diffraction (XRD) pattern shown in Fig. S1 indicates that the sintering process does not affect the phase composite of the pure LAGP. Additionally, the pristine LAGP film shows a relatively smooth surface and its cross-sectional surface is also compact (Fig. S2). Compared with the polished LAGP film, the cross-sectional SEM images of DSCCE present show the obvious sandwich structure in which two uniform interfacial layers are anchored on each side of LAGP ceramic: the thickness of the PMMA-based coating is ~150 μm and the thickness of the PVDF-HFP-based coating is ~50 μm, respectively (Fig. 1e–g).

It is well known that LiI has been widely used as the redox mediator (RM) in Li–air batteries since the I^-/I_3^- conversion can effectively promote the decomposition of discharge products in Li-air cells [51,52]. Nevertheless, the serious shuttle effect of soluble I-based species greatly discounts its RM role in liquid electrolyte (LE)-based Li–air cells. To clarify the inhibiting effect of the hybrid electrolyte on shuttle effect of soluble I-based species, the permeation tests for the DSCCE and Celegard membranes were carried out by using I_3^- as the color indicator (Fig. 2a and b). As shown in Fig. 2a, the color indicator I_3^- can go through the commercial separator after only 1 h and rapidly spread over the whole solution at the right side within 24 h, while the compact and uniform DSCCE layer can greatly suppress the I_3^- shuttle during 72 h (Fig. 2b). The UV–vis spectra results shown in Fig. S3 also confirm that DSCCE can effectively inhibit the soluble I-based specie shuttle. The resistibility towards O_2^- species of the polymer skeletons at both sides of DSCCE was further studied through Fourier transform infrared (FT-IR) spectra. It can be observed from Fig. 2c that when treated with KO_2 (KO_2 can release O_2^- species in 18-crown-6 containing TEGDME solution which have been considered as the main reaction intermediates for the Li–O_2 cells), there are not new peaks formed or original bands disappeared in the FT-IR spectra of PMMA, indicating that the O_2^- species almost have no influence on the polymer matrix of the PMMA-based coating layer. However, the FT-IR spectra shown in Fig. S4 suggest that PVDF-HFP is not very stable towards KO_2. These results confirm that the PMMA should be the optimized cathode-friendly polymer framework for Li–air batteries. On the other hand, to clarify the anode-friendly property of the PVDF-HFP coating, the PVDF-HFP-based symmetrical polymer coating ceramic-based composite electrolyte (SPCCE) is designed and further assembled in Li-based half cells possessing holes to allow ambient air to flow in (please see Fig. S5 for detail). For comparison, the LE is applied in the same batteries and tested under the same conditions. It can be found from Fig. S5a that the ambient air can easily go through the LE-dipped separator and react with the Li anodes and electrolytes of the battery. However, the SPCCE is so compact and robust that the ambient air almost cannot penetrate into the battery, and thus the Li electrodes and electrolyte of the corresponding cell are relatively stable (Fig. S5b). Because of the above fact, the voltage profiles of the SPCCE-based cell are very stable and its corresponding discharge/charge overpotentials are always around 0.10 V during 10,000 min, while the battery using LE can only normally work for about 500 min and its voltage polarization even can reach >0.84 V after 12 cycles (Fig. 2d and e). More interestingly, the overpotentials of the PMMA-modified LAGP (PMMA-SPCCE) based symmetric cell are also higher than these of PVDF-HFP-modified LAGP (SPCCE) based battery (Fig. S6), suggesting that the PVDF-HFP shows the better affinity towards metallic Li compared with the PMMA. Additionally, the electrochemical impedance spectroscopy (EIS) profiles of the SPCCE or LE-based symmetric cells at different cycles are also investigated (Fig. 2f and Tab. S1). Before cycling, the interface resistances (IRs) of the SPCCE or LE-containing batteries are 232.9 and 262.2 Ω, respectively. After 20 cycles, the IR of the cell with SPCCE can maintain around 195.0 Ω, but the IR of the battery using LE obviously increases to 484.1 Ω, suggesting that SPCCE can inhibit the uncontrollable dendrite Li growth and the rapidly air-attacking over cycling. These results demonstrate that PVDF-HFP/LAGP composite layer is beneficial to Li plating/stripping behavior in the ambient air. The thermogravimetric analysis (TGA) profiles of DSCCE and LE-based commercial separator present that the basic framework of DSCCE can be retained even at high-temperature, but the LE-dipped membrane is almost completely gone at ~500 °C, which is in agreement with the combustion experiments (Fig. 2g and S7). These imply the high safety and excellent heat stability of DSCCE. Fig. 2h shows that the ionic conductivity of DSCCE can reach 0.30 mS cm^{-1}, which is very close to that of LE (0.71 mS cm^{-1}, the ionic conductivity test is summarized in the experimental section of supporting information). The linear sweep voltammogram (LSV) profiles of the DSCCE and LE were also conducted to verify their electrochemical stability (Fig. 2i). The DSCCE composite electrolyte displays a wide electrochemical window above 5.0 V, which is much higher than that of LE. Moreover, the leakage test of the DSCCE and LE-dipped commercial separator further confirm that the DSCCE film can effectively address the leaking problem that usually occurs in LE-based Li batteries (Fig. S8). The collective results presented above indicate that the implementation of differentiating bilateral coatings on LAGP makes it an ideal electrolyte for Li–air batteries.

To further verify the advantage of the differentiating surface-modified ceramic, the Li–air batteries were assembled by using a carbon nanotube (CNT)-based cathode coupled with a Li metal anode in DSCCE or LE electrolyte (Fig. 3a, all these Li–air cells are operated in ambient air). Fig. 3b gives the voltage profiles of the DSCCE or LE-based Li–air cells under full discharge/charge conditions at 500 mA g^{-1}. As shown in Fig. 3b, the initial specific capacity of the Li–air battery using DSCCE is 11,836 mA h g^{-1} at 500 mA g^{-1} which is higher than LE-based cell (10,035 mA h g^{-1}) and several previously reported solid-state Li-air cells (Fig. 3g and Tab. S2). Additionally, the coulombic efficiency (CE) of DSCCE-based cell (~94.0%) is also higher than that of LE-based battery (~91.4%), while its average discharge/charge overpotential is

Please cite this article as: Y. Shi et al., Design of multifunctional interfaces on ceramic solid electrolytes for high-performance lithium-air batteries, Green Energy & Environment, https://doi.org/10.1016/j.gee.2024.02.010

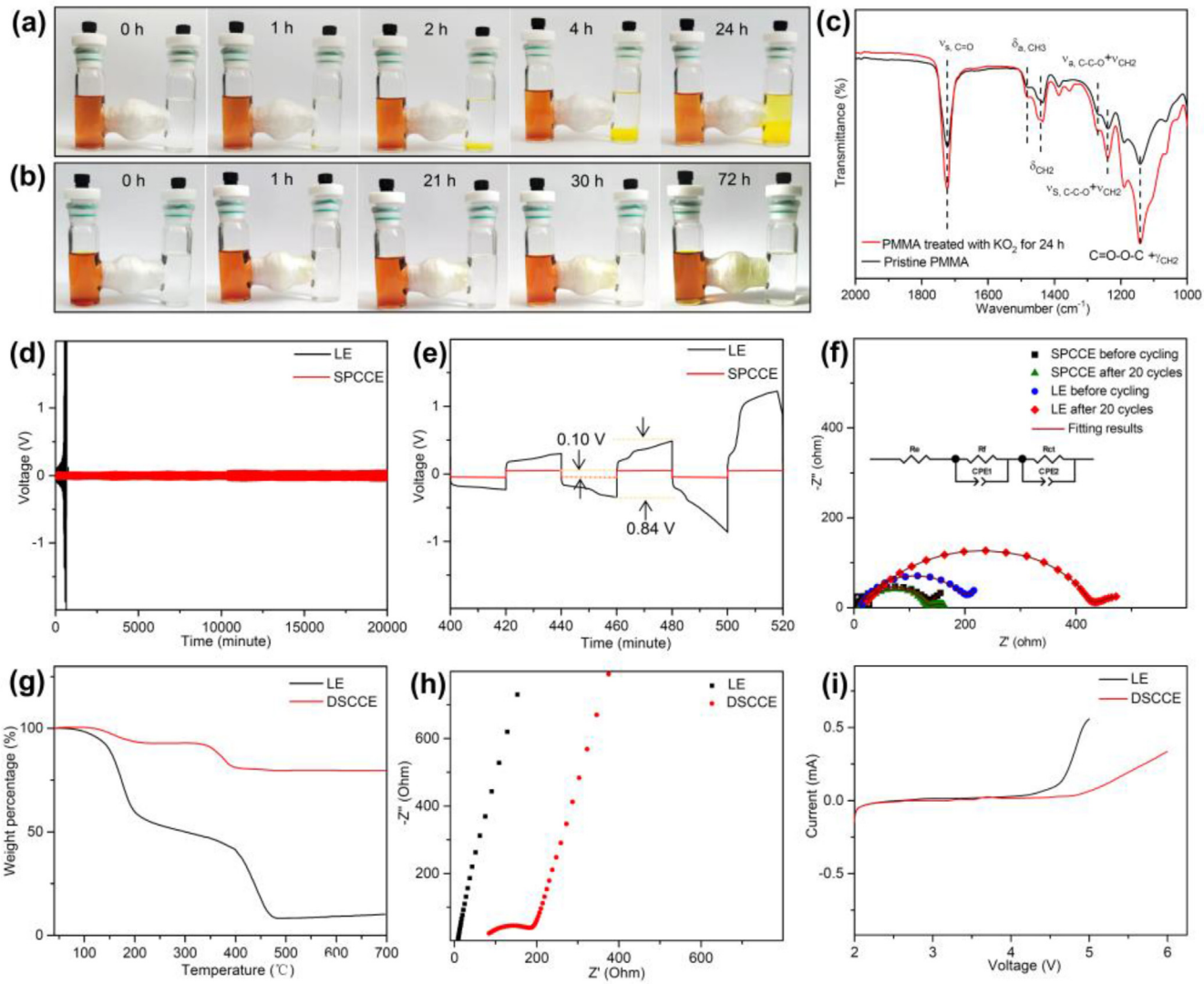

Fig. 2. Penetration test of the (a) Celegard membrane and (b) DSCCE film in the LiTFSI/TEGDME electrolyte with soluble I_3^- (color indicator); (c) FT-IR spectra of the pristine and reacted PMMA (treated with KO_2 +18-crown-6 in TEGDME for 24 h); (d) Continuous discharge/charge curves and (e) enlarged voltage profiles at 11-13th cycles of the SPCCE or LE based symmetric cells at 0.3 mA cm^{-2} with the limited capacity of 0.1 mAh cm^{-2} with the existence of ambient air; (f) EIS plots of the symmetrical batteries using SPCCE or LE exposed to air at different cycles (the detailed structure of these symmetrical cells is shown in supporting information); (g) TGA of DSCCE film and Celegard membrane dipped with LE, (h) Nyquist plots (in the stainless steel (SS)/electrolyte/SS cell structure) and (i) LSV profiles (in the SS/electrolyte/Li battery structure) of DSCCE and LE.

~1.45 V that is also obviously lower than the cell utilizing LE (~1.86 V). Moreover, the rate capabilities of the Li–air batteries using DSCCE or LE were also studied (Fig. 3c and S9-10). It can be seen that the discharge capacity retention rates of the cells utilizing DSCCE at 500 and 1000 mA g^{-1} are as high as 85.8 and 68.2% (based the capacity at 250 mA g^{-1}), while the capacity retention percentages of LE-based batteries are only 67.0 and 39.6%, respectively. These results indicate that DSCCE can effectively improve the capacity and rate performances of Li–air batteries. Moreover, the continuous discharge/charge measurements at fixed capacity for the DSCCE or LE based Li–air batteries were also carried out to evaluate their cycling stability. The Li–air cell using LE only normally works for <40 cycles and its charge terminal voltages rapidly increase to 5 V when cycled at 750 mA g^{-1} with the limited capacity of 750 mAh g^{-1} (Fig. 3d). Nevertheless, the DSCCE-based cell can stably operate for ~300 cycles, which is much better than LE-containing battery and recently reported polymer/solid-state Li–air cells (Fig. 3e and h and Tab. S2). Especially, the average discharge/charge overpotentials of the Li–air cell using DSCCE (~1.94 V) are lower compared with the cell utilizing LE (~2.47 V) over cycling (Fig. 3f), which indicate that the combination of LiI redox mediator and compact solid electrolyte film can effectively reduce the charge polarizations and also enhance the cycling performance of the Li-air batteries. Even at the higher discharge/charge depth (with the limited capacity of 1500 mAh g^{-1}), the Li–air battery with DSCCE can still display the relatively stable discharge/charge curves over 100 cycles (Fig. 3i and S11). These results have further

Please cite this article as: Y. Shi et al., Design of multifunctional interfaces on ceramic solid electrolytes for high-performance lithium-air batteries, Green Energy & Environment, https://doi.org/10.1016/j.gee.2024.02.010

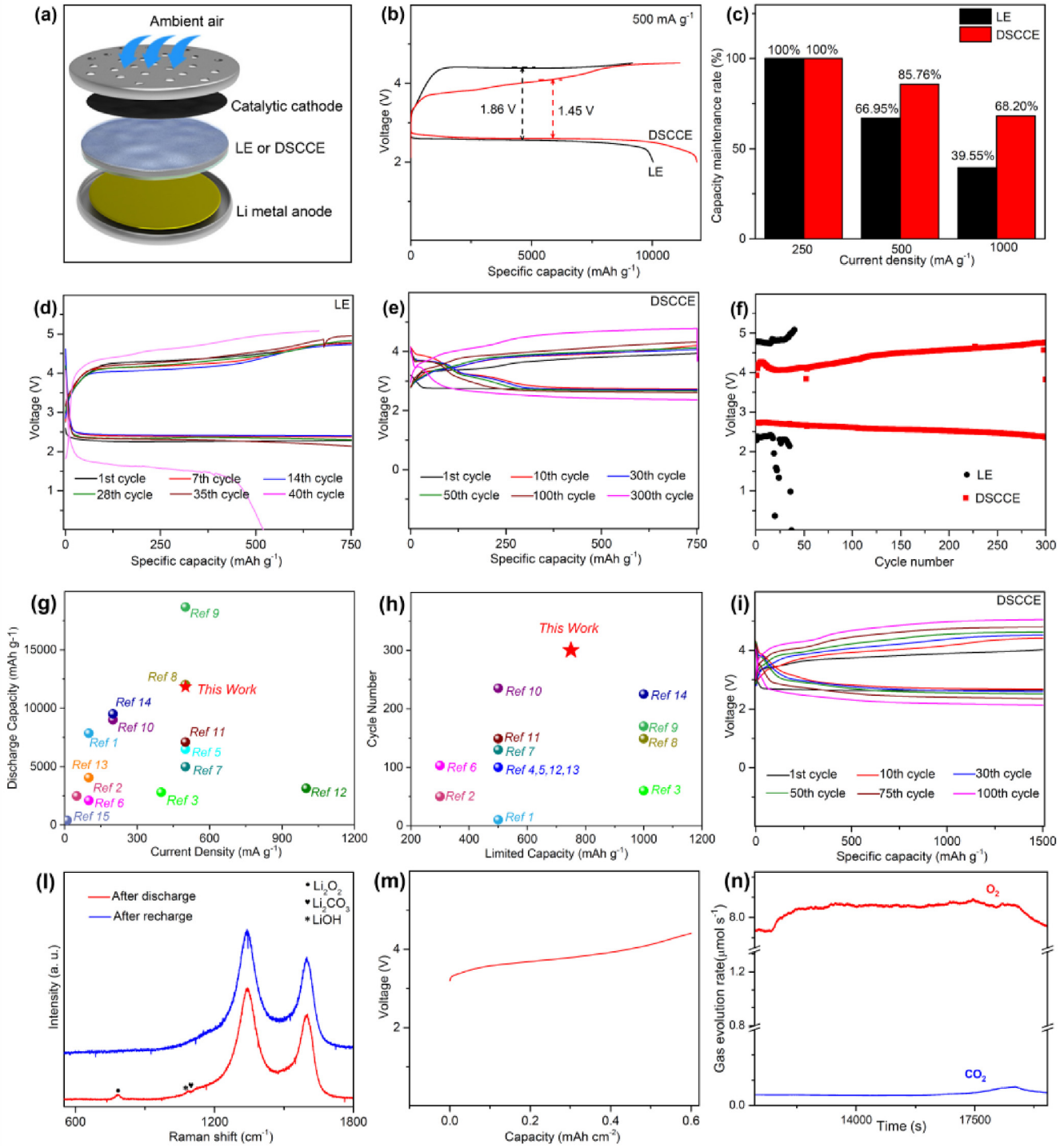

Fig. 3. (a) Schematic of the detailed composition for the Li–air battery using DSCCE or LE in ambient air; (b) Discharge/charge profiles at 500 mA g^{-1} and (c) capacity retention rates at different currents of the DSCCE or LE based Li–air full cells under full discharge/charge conditions; Voltage curves at various cycles of the Li–air batteries using (d) LE or (e) DSCCE at 750 mA g^{-1} with capacity of 750 mAh g^{-1}, and (f) their corresponding terminal voltages over the discharge/charge process; Comparison of (g) discharge capacities and (h) cycling life of the DSCCE based Li–air cells with the recently reported solid-state Li–O_2 batteries (Ref. 1–15 has been given in the references of Supporting Information (corresponding to ref. S1-15)); (i) Cycling performance of the DSCCE based Li–air cell at 750 mA g^{-1} with the higher fixed capacity of 1500 mAh g^{-1}; (l) Raman spectra of the discharged and recharged cathodes in DSCCE-based Li–air cells; (m) Charge profile and (n) corresponding *in-situ* DEMS data of the DSCCE-based Li–air battery at the constant current of 0.3 mA cm^{-2} with the fixed capacity of 0.6 mAh cm^{-2}.

Please cite this article as: Y. Shi et al., Design of multifunctional interfaces on ceramic solid electrolytes for high-performance lithium-air batteries, Green Energy & Environment, https://doi.org/10.1016/j.gee.2024.02.010

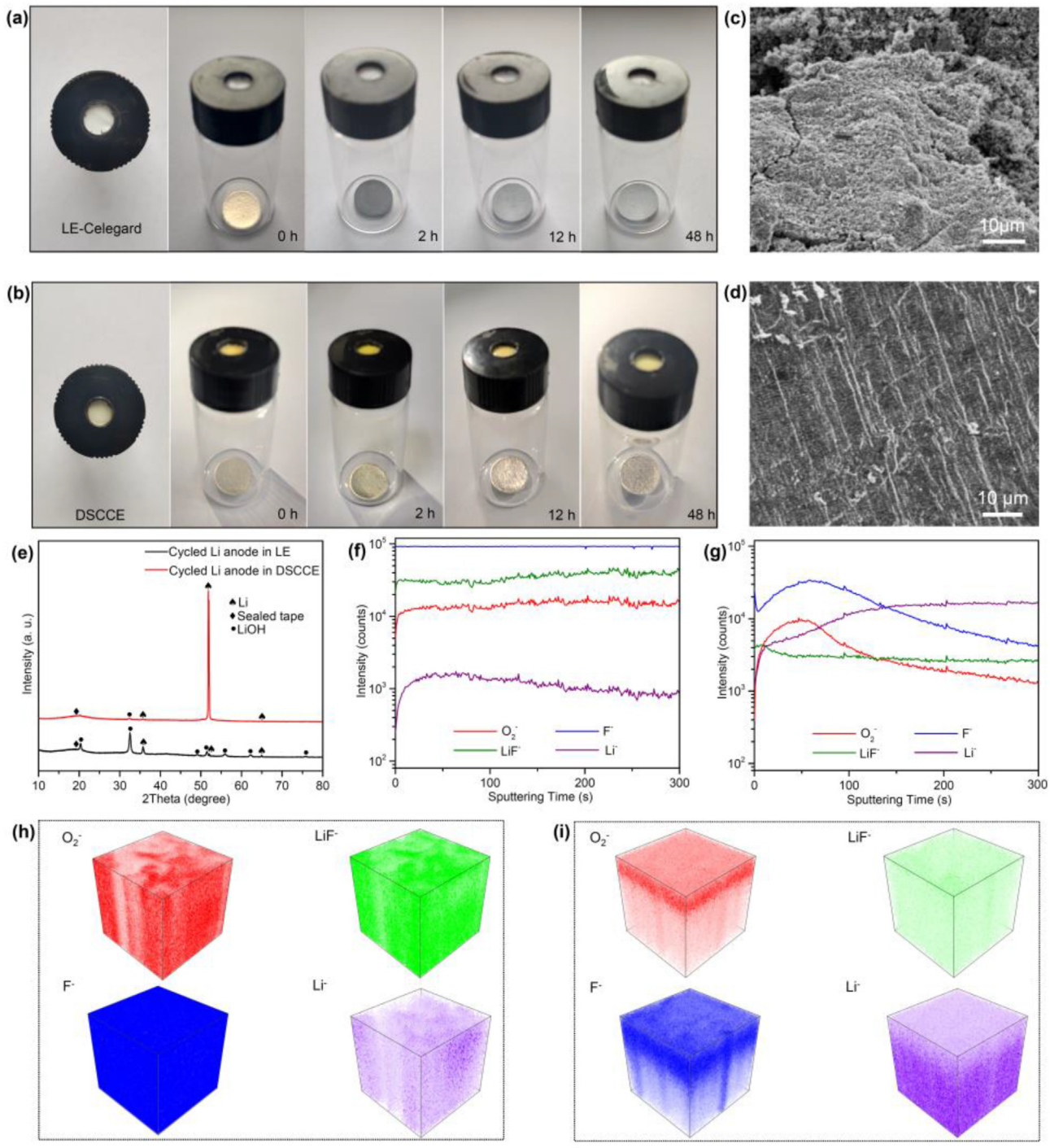

Fig. 4. The time-resolved surface evolution of Li anodes that are stored in the home-made testing bottles sealed with (a) LE-dipped Celegard or (b) DSCCE membranes; Surface SEM images of the cycled Li anodes in Li–air batteries using (c) LE or (d) DSCCE; (e) XRD patterns of the Li metal electrodes in LE or DSCCE based Li–air cells after 30 cycles; (f, g) TOF-SIMs depth profiles and (h, i) 3D reconstruction images corresponding to the SIMS intensity varying with the etching depth of some typical chemical ions for the cycled Li derived from the Li–air cells using (f, h) LE or (g, i) DSCCE.

demonstrated that LiI-PMMA coating layer can effectively enhance the battery reversibility. The Raman data shown in Fig. 3l present that an obvious peak at ~790 cm^{-1} assigned to Li_2O_2 and a weak band at around 1090 cm^{-1} attributed to Li_2CO_3/LiOH can be observed after discharge which indicate that the main discharge product is Li_2O_2 which is accompanied by Li_2CO_3/LiOH in this battery. Furthermore, all these peaks are disappeared on the recharged cathode. To further clarify the gas products overcharge, the homemade DSCCE-based Li–air battery was detected by the in situ differential electrochemical mass spectroscopy (DEMS) technology (Fig. 3m and n). As shown in Fig. 3m, the average charge potential of this DSCCE-based Li-air cell is below 4.0 V at 0.3 mA cm^{-2} with the limited capacity of 0.6 mAh cm^{-2},

Please cite this article as: Y. Shi et al., Design of multifunctional interfaces on ceramic solid electrolytes for high-performance lithium-air batteries, Green Energy & Environment, https://doi.org/10.1016/j.gee.2024.02.010

further confirming the important roles of the multi-functional DSCCE in Li-air cells. Moreover, it can be found from Fig. 3n that its main gas product is O_2 over charging, which is accompanied by a small amount of CO_2 that may be derived from Li_2CO_3 induced by the ambient air or electrolyte-related side reactions. Moreover, the *ex-situ* SEM images of the air cathodes at different stages show that the spherical products are formed around the CNTs after discharge and then vanish during the following charge process (Fig. S12). These solid proofs suggest that the good electrolyte–electrode contacts (PMMA|air cathode and PVDF-HFP|Li anode), high oxidative stability of PMMA, good compatibility towards Li of PVDF-HFP and RM role of LiI in the DSCCE can effectively improve the reversibility of the Li–air battery.

To better understand the superior electrochemical properties of the DSCCE-based Li–air cells in ambient air, a series of characterizations were conducted. Fig. 4a and b presents the protective effects of the DSCCE and LE-dipped commercial separator on Li anodes in ambient air. The Li film that are stored in the DSCCE-sealed bottle can keep its originally metal luster over 48 h resting, but the surface color of the metallic Li rapidly turned black after only 2 h and eventually changed into white within 12 h aging (Fig. 4a and b). These results indicate that the DSCCE film is so compact that it can obviously inhibit the air-attacking on Li anodes. The Li anodes in the Li–air cells with DSCCE or LE after cycling are also systemically investigated to verify the advantages of DSCCE. Firstly, the SEM images of the cycled Li anodes protected by DSCCE or LE in Li–air batteries are given in Fig. 4c and d. As shown in Fig. 4c, the cycled Li anode in LE-based battery display the very rough surface with many apparent cracks, indicating that metallic Li anode is seriously corroded and many dead Li metals separated from the Li electrode bulk are formed during cycling. On the contrast, the Li electrode after 30 cycles in the DSCCE-based cell still exhibits the relatively flat and compact surface which is very different from the cycled Li anode in LE-based battery (Fig. 4d). Additionally, the XRD patterns shown in Fig. 4e suggest that there is a broad peak at ~20° and several typical bands located at around 36°, 52° and 65° in both Li anodes cycled in the LE or DSCCE containing Li–air cells, which are assigned to the sealing membrane (Fig. S13) and metallic Li (JCPDS 15-0401), respectively. In addition to the above peaks, the LiOH phase can be also apparently observed in the XRD patterns of the cycled Li of the LE-based Li–air cell, but the corresponding LiOH peaks are almost negligible in the cycled Li of the battery using DSCCE. The Time-of-flight secondary ion mass spectrometry (TOF-SIMS) measurements are also carried out to detect the surface evolution of Li anodes in Li–air batteries using DSCCE or LE over cycling (Fig. 4f–i). It is well known that the decomposition of organic solvent/Li salt and the attacking of O_2^- on the Li anodes during cycling can generate a lot of side products, such as F, O or Li-containing species. It can be seen from the SIMS depth curves and corresponding 3D reconstruction images shown in Fig. 4f and h that the contents of O_2^-, F^- and LiF^- on the surface of the cycled Li electrode are relatively stable over the whole sputtering process. However, it should be noted that the signal of F^- in Fig. 4f is so strong that exceeded the detection limit of a device [53]. Hence, the F_2^- species are also analyzed by the TOF-SIMS technology since both F^- and F_2^- species can represent the variation trend of F elements in the surface passivation layer. The concentration change of F_2^- is similar to these of O_2^- and LiF^- ions on the reacted Li anode in LE-based cells (Fig. S14). These indicate that the surface passivation layer is very thick and the corresponding side reactions are serious on the cycled Li anode of the Li–air cell using LE over cycling. In contrast, all the signals of O_2^-, F^- (or F_2^-) and LiF^- from the cycled Li electrode in DSCCE-based battery show a decreasing trend with the rise of sputtering time (Fig. 4g and i). Additionally, all the surface contents of these ions on the cycled Li anode of the DSCCE-based Li–air battery are obviously lower than these of corresponding ions on the cycled Li electrode of the LE-based Li–air cell. Moreover, the content of Li^- from the cycled Li electrode of the DSCCE-based Li–air battery significantly rise as the etching time increases, which is much higher than that on anode in LE-based Li–air cell (Fig. 4f–i). These phenomena demonstrate that the compact and uniform DSCCE composite layer can effectively inhibit the side reactions on Li anode during cycling. In total, for DSCCE, the LiI-containing PMMA modified layer can greatly inhibit O_2^--induced side reactions and also reduce charge overpotentials. Moreover, the PVDF-HFP modification layer can show the excellent affinity towards metallic Li and obviously reduce the interface resistance between LAGP and Li anode. Therefore, DSCCE can effectively promote the electrochemical performance of Li-air batteries.

4. Conclusion

In summary, the PMMA-based layer with LiI redox mediator and the PVDF-HFP-based coating were fabricated on the LAGP pellet through the UV treatment as the cathode- and anode-friendly interfaces for Li–air batteries, respectively. The robust and compact ceramic/polymer layer can effectively suppress the infinite dendritic Li growth/electrode dimension change and also prevent Li anode from air or I-based species attacking. In addition, the anti-oxidative PMMA-based coating greatly reduce the O_2^- induced side reactions, while the PVDF-HFP-based layer obviously reduce the interface impedance between LAGP and anode. Moreover, the LiI additives can act as the redox mediator (RM) to realize the small charge potential polarization and the high ionic conductivity of the composite electrolyte also is beneficial to the electrochemical reactions in batteries. When operated at full discharge/charge condition, the Li–air cells using DSCCE display the extra-high capacity of 11,836 mA h g^{-1} at 500 mA g^{-1} with low average overpotentials of 1.45 V, superior capacity retention (the discharge capacity at 1000 mA g^{-1} is as high as 68.2 % of the capacity at 250 mA g^{-1}). When working under the limited capacity of 750 mAh g^{-1}, the DSCCE based Li–air battery shows the ultra-long cycling life (~300 cycles at 750 mA g^{-1}), which is

Please cite this article as: Y. Shi et al., Design of multifunctional interfaces on ceramic solid electrolytes for high-performance lithium-air batteries, Green Energy & Environment, https://doi.org/10.1016/j.gee.2024.02.010

much better than the LE-based cells (normally operate for <40 cycles). Even under the deeper limited capacity (1500 mAh g^{-1}), the corresponding cell using DSCCE still presents the superior cycling stability (100 cycles). The new DSCCE with typical three-tier structure pave the new way for the development of the composite electrolytes that are crucial for the high-performance Li–air batteries.

CRediT authorship contribution statement

Yunxin Shi: Writing – original draft, Software, Methodology, Formal analysis, Data curation. **Ziyang Guo:** Writing – review & editing, Writing – original draft, Supervision, Methodology, Investigation, Funding acquisition, Formal analysis, Conceptualization. **Changhong Wang:** Writing – review & editing, Software, Formal analysis, Data curation. **Mingze Gao:** Validation, Software, Data curation. **Xiaoting Lin:** Investigation, Formal analysis, Data curation. **Hui Duan:** Software, Formal analysis, Data curation. **Yonggang Wang:** Writing – review & editing, Supervision, Resources, Investigation. **Xueliang Sun:** Writing – review & editing, Supervision, Project administration, Investigation, Funding acquisition, Conceptualization.

Conflict of interest

There are no conflicts to declare.

Acknowledgements

This research was supported by the National Natural Science Foundation of China (22379074), Young Science and Technology Talent Program of Inner Mongolia Province (NJYT24001), Natural Sciences and Engineering Research Council of Canada (NSERC), GLABAT Solid-State Battery Inc., China Automotive Battery Research Institute Co. Ltd, Canada Research Chair Program (CRC), Canada Foundation for Innovation (CFI), and Ontario Research Fund. Z. Y. G. was supported by the Chinese Scholarship Council.

Appendix A. Supplementary data

Supplementary data to this article can be found online at https://doi.org/10.1016/j.gee.2024.02.010.

References

[1] H. Wang, D.D. Yu, C.W. Kuang, L.W. Cheng, W. Li, X.L. Feng, Z. Zhang, X.B. Zhang, Y. Zhang, Chem 5 (2019) 313–338.
[2] J.W. Liang, X.N. Li, K.R. Adair, X.L. Sun, Acc. Chem. Res. 54 (2021) 1023–1033.
[3] H. Pan, M.H. Zhang, Z. Cheng, H.Y. Jiang, J.G. Yang, P.F. Wang, P. He, H.S. Zhou, Sci. Adv. 8 (2022) eabn4372.
[4] Y. Liu, W. Li, Y.Y. Xia, Electrochem. Energy Rev. 4 (2021) 447–472.
[5] Y. Chen, S.Z. Liu, Z.X. Bi, Z. Li, F.Y. Zhou, R.F. Shi, T.C. Mu, Green Energy Environ. (2024), https://doi.org/10.1016/j.gee.2023.05.002.
[6] H. Yang, B. Zhang, M.X. Jing, X.Q. Shen, L. Wang, H. Xu, X.H. Yan, X.M. He, Adv. Energy Mater. 12 (2022) 2201762.
[7] K.C. Pan, M.h. Li, W.C. Wang, S.C. Xing, Y.Y. Dou, S.S. Gao, Z. Zhang, Z. Zhou, Green Energy Environ. 8 (2023) 939e944.
[8] T.T. Dong, P.Z. Mu, S. Zhang, H.R. Zhang, W. Liu, G.L. Cui, Electrochem. Energy Rev. 4 (2021) 545–565.
[9] S.M. Xu, X. Liang, X. Liu, W.L. Bai, Y.S. Liu, Z.P. Cai, Q. Zhang, C. Zhao, K.X. Wang, J.S. Chen, Energy Storage Mater. 25 (2020) 52–61.
[10] H. Ouyang, S. Min, J. Yi, X.Y. Liu, F.H. Ning, J.Q. Qin, Y. Jiang, B. Zhao, J.J. Zhang, Green Energy Environ. 8 (2023) 1195e1204.
[11] Z.H. Huang, J. Li, L.X. Li, H.M. Xu, C. Han, M.Q. Liu, J. Xiang, X.Q. Shen, M.X. Jing, Ceram. Int. 48 (2022) 25949.
[12] Z.J. Liu, G.Q. Liu, L.L. Cheng, J. Gu, H.R. Yuan, Y. Chen, Y.F. Wu, Green Energy Environ. (2024), https://doi.org/10.1016/j.gee.2023.09.001.
[13] H. Ouyang, S. Min, J. Yi, X. Liu, F.H. Ning, Y. Xu, Y. Jiang, B. Zhao, J.J. Zhang, ACS Appl. Mater. Interfaces 14 (2022) 53648–53657.
[14] R. Li, J. Li, L.X. Li, H. Yang, G. Zhang, J. Xiang, X.Q. Shen, M.X. Jing, Colloids Surf., A 657 (2023) 130600.
[15] X.W. Chi, M.L. Li, J.C. Di, P. Bai, L.N. Song, X.X. Wang, F. Li, S. Liang, J.J. Xu, J.H. Yu, Nature 592 (2021) 551–557.
[16] P. Wang, D.Y. Zhao, X.B. Hui, Z. Qian, P. Zhang, Y.Y. Ren, Y. Lin, Z.W. Zhang, L.W. Yin, Adv. Energy Mater. 11 (2021) 2003069.
[17] Y. Zhou, K. Yin, Q.F. Gu, L. Tao, Y.J. Li, H. Tan, J.H. Zhou, W.S. Zhang, H.B. Li, S.J. Guo, Angew. Chem. Int. Ed. 60 (2021) 26592–26598.
[18] Y.Y. Dou, Z.J. Xie, Y.J. Wei, Z.Q. Peng, Z. Zhou, Natl. Sci. Rev. 9 (2022) nwac040.
[19] J.Q. Zhang, Y.F. Zhao, B. Sun, Y. Xie, A. Tkacheva, F.L. Qiu, P. He, H.S. Zhou, K. Yan, X. Guo, S.J. Wang, A.M. McDonagh, Z.Q. Peng, J. Lu, G.X. Wang, Sci. Adv. 8 (2022) eabm1899.
[20] S.Y. Ma, H.C. Yao, Z.J. Li, Q.C. Liu, J. Energy Chem. 70 (2022) 614–622.
[21] S.C. Wu, J. Yi, K. Zhu, S.Y. Bai, Y. Liu, Y. Qiao, M. Ishida, H.S. Zhou, Adv. Energy Mater. 7 (2017) 1601759.
[22] J. Lu, Z.W. Chen, F. Pan, Y. Cui, K. Amine, Electrochem. Energy Rev. 1 (2018) 35–58.
[23] Y.X. Wang, Y.J. Liu, M. Nguyen, J. Cho, N. Katyal, B.S. Vishnugopi, H.C. Hao, R.Y. Fang, N. Wu, P.C. Liu, P.P. Mukherjee, J. Nanda, G. Henkelman, J. Watt, D. Mitlin, Adv. Mater. 35 (2023) 2206762.
[24] W. Liang, F. Lian, N. Meng, J.H. Lu, L.J. Ma, C.-Z. Zhao, Q. Zhang, Energy Storage Mater. 28 (2020) 350–356.
[25] C.L. Li, G. Huang, Y. Yu, Q. Xiong, J.M. Yan, X.B. Zhang, J. Am. Chem. Soc. 144 (2022) 5827–5833.
[26] X.H. Zou, Q. Lu, K.M. Liao, Z.P. Shao, Energy Storage Mater. 45 (2022) 869–902.
[27] S. Gu, C.Z. Sun, D. Xu, Y. Lu, J. Jin, Z.Y. Wen, Electrochem. Energy Rev. 1 (2018) 599–624.
[28] X.W. Pan, J.W. Sun, C. Jin, Z.J. Wang, R.J. Xiao, L. Peng, L.W. Shen, C. Li, R.Z. Yang, Solid State Ionics 351 (2020) 115340.
[29] C.W. Wang, K. Fu, S.P. Kammampata, D.W. McOwen, A.J. Samson, L. Zhang, G.T. Hitz, A.M. Nolan, E.D. Wachsman, Y.F. Mo, V. Thangadurai, L.B. Hu, Chem. Rev. 120 (2020) 4257–4300.
[30] J.N. Lai, Y. Xing, N. Chen, L. Li, F. Wu, R.J. Chen, Angew. Chem. Int. Ed. 59 (2020) 2974–2997.
[31] Z.W. Zhao, L. Pang, Y.Y. Mu, Y.Z. Chen, Z.Q. Peng, Adv. Energy Mater. 13 (2023) 2301127.
[32] Y.B. Kim, I.T. Kim, M.J. Song, M.W. Shin, J. Membr. Sci. 563 (2018) 835–842.
[33] E. Umeshbabu, B.Z. Zheng, Y. Yang, Electrochem. Energy Rev. 2 (2019) 199–230.
[34] L.L. Liu, H.P. Guo, L.J. Fu, S.L. Chou, S. Thiele, Y.P. Wu, J.Z. Wang, Small 17 (2019) 1903854.
[35] M.L. Xie, Z.M. Huang, X. Lin, Y.K. Li, Z.M. Huang, L.X. Yuan, Y. Shen, Y.H. Huang, Energy Storage Mater. 20 (2019) 307–314.
[36] A. Kondori, M. Esmaeilirad, A.M. Harzandi, R. Amine, M.T. Saray, L. Yu, T.C. Liu, J.G. Wen, N.N. Shan, H.H. Wang, A.T. Ngo, P.C. Redfern, C.S. Johnson, K. Amine, R. Shahbazian-Yassar, L.A. Curtiss, M. Asadi, Science 379 (2023) 499–505.
[37] M.Y. Jia, N. Zhao, H.Y. Huo, X.X. Guo, Electrochem. Energy Rev. 3 (2020) 656–689.
[38] H. Su, Y. Liu, Y. Zhong, J.R. Li, X.L. Wang, X.H. Xia, C.D. Gu, J.P. Tu, Nano Energy 96 (2022) 107104.

[39] J.K. Hu, H. Yuan, S.J. Yang, Y. Lu, S. Sun, J. Liu, Y.L. Liao, S. Li, C.Z. Zhao, J.Q. Huang, J. Energy Chem. 71 (2022) 612–618.
[40] C.H. Wang, J.W. Liang, J. Luo, J. Liu, X.N. Li, F.P. Zhao, R.Y. Li, H. Huang, S.Q. Zhao, L. Zhang, J.T. Wang, X.L. Sun, Sci. Adv. 7 (2021) eabh1896.
[41] H. Kwak, S. Wang, J. Park, Y.S. Liu, K.T. Kim, Y. Choi, Y.F. Mo, Y.S. Jung, ACS Energy Lett. 7 (2022) 1776–1805.
[42] Y.M. Du, Y.J. Liu, S.X. Yang, C. Li, Z. Cheng, F.L. Qiu, P. He, H.S. Zhou, J. Mater. Chem. A 9 (2021) 9581–9585.
[43] X.W. Yu, L.G. Xue, J.B. Goodenough, A. Manthiram, Adv. Funct. Mater. 31 (2021) 2002144.
[44] R. Zhao, L. Gao, M.R. Song, Y. Ye, Z.B. Liang, J.C. Bian, J.L. Zhu, S. Li, R.Q. Zou, Y.S. Zhao, ACS Energy Lett. 6 (2021) 3141–3150.
[45] A. Paolella, X. Liu, A. Daali, W.Q. Xu, I. Hwang, S. Savoie, G. Girard, A.G. Nita, A. Perea, H. Demers, W. Zhu, A. Guerfi, A. Vijh, G. Bertoni, G.C. Gazzadi, G. Berti, C.J. Sun, Y. Ren, K. Zaghib, M. Armand, C. Kim, G.L. Xu, K. Amine, Adv. Funct. Mater. 31 (2021) 2102765.
[46] A. Paolella, W. Zhu, G.L. Xu, A.L. Monaca, S. Savoie, G. Girard, A. Vijh, H. Demers, A. Perea, N. Delaporte, A. Guerfi, X. Liu, Y. Ren, C.J. Sun, J. Lu, K. Amine, K. Zaghib, Adv. Energy Mater. 10 (2020) 2001497.
[47] H. Duan, M. Fan, W.P. Chen, J.Y. Li, P.F. Wang, W.P. Wang, J.L. Shi, Y.X. Yin, L.J. Wan, Y.G. Guo, Adv. Mater. 31 (2019) 1807789.
[48] Z. Cheng, H. Pan, F. Li, C. Duan, H. Liu, H.Y. Zhong, C.C. Sheng, G.J. Hou, P. He, H.S. Zhou, Nat. Commun. 13 (2022) 125.
[49] J.Y. Liang, X.X. Zeng, X.D. Zhang, T.T. Zuo, M. Yan, Y.X. Yin, J.L. Shi, X.W. Wu, Y.G. Guo, L.J. Wan, J. Am. Chem. Soc. 141 (2019) 9165–9169.
[50] C.T. Zhao, Y.M. Zhu, Q. Sun, C.H. Wang, J. Luo, X.T. Lin, X.F. Yang, Y. Zhao, R.Y. Li, S.Q. Zhao, H. Huang, L. Zhang, S.G. Lu, M. Gu, X.L. Sun, Angew. Chem. Int. Ed. 60 (2021) 5821–5826.
[51] X.P. Zhang, Y.Y. Sun, Z. Sun, C.S. Yang, T. Zhang, Nat. Commun. 10 (2019) 3543.
[52] Z.Y. Guo, Q.W. Zhang, C. Wang, Y.J. Zhang, S.M. Dong, G.L. Cui, Adv. Funct. Mater. 32 (2022) 2108993.
[53] C.W. Ma, F. Xu, T.L. Song, ACS Appl. Mater. Interfaces 14 (2022) 20197–20207.

Please cite this article as: Y. Shi et al., Design of multifunctional interfaces on ceramic solid electrolytes for high-performance lithium-air batteries, Green Energy & Environment, https://doi.org/10.1016/j.gee.2024.02.010